

# Dark MaGICC: the effect of Dark Energy on galaxy formation. Cosmology does matter.

C. Penzo<sup>1\*</sup>, A.V. Macciò<sup>1</sup>, L. Casarini<sup>2</sup>, G. S. Stinson<sup>1</sup>, J. Wadsley<sup>3</sup>

<sup>1</sup> *Max-Planck-Institut für Astronomie, Königstuhl 17, 69117 Heidelberg, Germany*

<sup>2</sup> *Departamento de Física, Universidade Federal do Espírito Santo, Av. Fernando Ferrari 514, 29075-910 Vitória (ES), Brazil*

<sup>3</sup> *Department of Physics and Astronomy, McMaster University, Hamilton, Ontario, L8S 4M1, Canada*

16 January 2014

## ABSTRACT

We present the Dark MaGICC project, which aims to investigate the effect of Dark Energy (DE) modeling on galaxy formation via hydrodynamical cosmological simulations. Dark MaGICC includes four dynamical Dark Energy scenarios with time varying equations of state, one with a self-interacting Ratra-Peebles model. In each scenario we simulate three galaxies with high resolution using smoothed particle hydrodynamics (SPH). The baryonic physics model is the same used in the Making Galaxies in a Cosmological Context (MaGICC) project, and we varied only the background cosmology. We find that the Dark Energy parameterization has a surprisingly important impact on galaxy evolution and on structural properties of galaxies at  $z = 0$ , in striking contrast with predictions from pure Nbody simulations. The different background evolutions can (depending on the behavior of the DE equation of state) either enhance or quench star formation with respect to a  $\Lambda$ CDM model, at a level similar to the variation of the stellar feedback parameterization, with strong effects on the final galaxy rotation curves. While overall stellar feedback is still the driving force in shaping galaxies, we show that the effect of the Dark Energy parameterization plays a larger role than previously thought, especially at lower redshifts. For this reason, the influence of Dark Energy parametrization on galaxy formation must be taken into account, especially in the era of precision cosmology.

**Key words:** cosmology: dark energy – galaxy: formation – galaxies: spiral – hydrodynamics – methods: numerical

## 1 INTRODUCTION

Since the first Type Ia Supernova data were published (Riess et al. 1998, Perlmutter et al. 1999), it has been clear that our Universe is expanding with a positive acceleration. To enable an accelerated expansion, there needs to be a repulsive force in our model of the Universe, and thus Einstein’s Cosmological Constant  $\Lambda$  was reintroduced. Its reintroduction lead to the current standard  $\Lambda$  Cold Dark Matter ( $\Lambda$ CDM) cosmological model.

Allowing the existence of a Cosmological Constant is the simplest solution to obtain a positive acceleration. It implies that more than 70% of the energy in our Universe could be described as a homogeneous fluid whose equation-

of-state parameter is  $w \equiv p/\rho = -1$  and, consequently, that its energy density  $\Omega_\Lambda$  remains constant as a function of time.

Despite the excellent agreement of  $\Lambda$ CDM cosmology with observations, the model does suffer from fundamental problems. The Cosmological Constant must be finely tuned in the early Universe to reproduce the fit to observations we see today. Moreover, the attempt to explain the presence of such an energy density with vacuum energy fails by several orders of magnitude in predicting today’s  $\Lambda$  energy density value. Finally it is a remarkable coincidence that the values of the energy densities of  $\Lambda$  and of matter are today of the same order (see Weinberg 1989, Carroll et al. 1992).

For these reasons cosmologists have been seeking alternatives to a Cosmological Constant. Such alternatives are generally referred to as “dark energy”, a more general setting in which the equation-of-state parameter  $w$  is allowed to be a function of time. Under this assumption, we describe dark

\* penzo@mpia.de

energy with a homogeneous scalar field whose energy density evolves with time. This changes the expansion history of the Universe and affects the evolution of density perturbations, Baldi (2012). Thus, distinctive signatures of dark energy models can be found by looking at the formation of structures.

In pioneering dark-matter-only simulations with an evolving  $w$ , Klypin et al. (2003) found that the differences between the cosmological models were not significant at  $z=0$  both in the non-linear matter power spectrum and in the halo mass function, although differences between models became significant at higher redshifts with a higher number of clusters for the dark energy models compared to  $\Lambda$ CDM.

Subsequently, multiple groups investigated the properties of dark matter structures in DE cosmologies (Dolag et al. 2004, Bartelmann et al. 2005 and Grossi & Springel 2009). They looked at halo concentrations, velocity dispersions and abundance relations in dark energy and early dark energy models. More significant differences on the halo mass functions between the  $\Lambda$ CDM and dark energy cosmologies were found at high redshifts (in these works, all models have the same value for the mean density amplitude  $\sigma_8$  at  $z=0$ ).

Several studies compared the inner structure of haloes simulated in  $\Lambda$ CDM and dark energy cosmologies in collisionless simulations. In all cases, a Navarro-Frenk-White (Navarro et al. 1997) density profile well described the matter distribution. The only difference in the dark energy simulations was that the matter was more centrally concentrated because the haloes had earlier formation times (Klypin et al. 2003; Linder & Jenkins 2003; Kuhlen et al. 2005).

While these studies all considered dark energy cosmologies that featured earlier collapse times than  $\Lambda$ CDM, it is also possible for dark energy cosmologies to form structure later. The equation-of-state parameter,  $w(a)$  can “cross over the Cosmological Constant boundary from below”. In other words,  $w$  can evolve from  $w < -1$  at high redshift to  $w > -1$  at  $z = 0$ . Such models have *less* collapsed structure at high redshift than  $\Lambda$ CDM. Xia et al. (2006) and Xia et al. (2013) showed observational constraints favor such models.

While it is useful to study collisionless simulations of dark energy cosmologies, we can only directly observe baryons. Even though they account for  $\sim \frac{1}{5}$  of the mass density of dark matter in the Universe, baryons can have an impact on the formation of small scale structures (White 1976; Zhan & Knox 2004; Puchwein et al. 2005; Jing et al. 2006; Rudd et al. 2008; Casarini et al. 2011b; De Boni et al. 2011; van Daalen et al. 2011; Casarini et al. 2012; Fedeli et al. 2012). So far, simulations including dark energy have focused on massive galaxy clusters since cosmology has the largest effect on the formation of the largest structures.

In the last decade different groups have been studying galaxy formation and evolution by performing high resolution hydrodynamical simulations in a cosmological context. Only recently they have succeeded in simulating realistic disk galaxies, e.g. star formation history matching with observational constraints, flat rotation curves, exponential surface density profiles (see Robertson et al. 2006, Governato et al. 2007, Agertz et al. 2011, Guedes et al. 2011, Brook et al. 2012, Scannapieco et al. 2012, Stinson et al. 2013a, Marinacci et al. 2013). In all of these high resolution simulations a  $\Lambda$ CDM cosmology has always been assumed. Recently an attempt to study galaxy formation in differ-

ent cosmological models has been presented in Fontanot et al. (2012, 2013), where Nbody simulations were combined with a Semi Analytical Model (SAM) for galaxy formation. While they were able to address the effect of cosmology on global properties of galaxies (e.g. the cosmic star formation), due to their approach they were not able to study the effects of Dark Energy parametrization on the internal structure of simulated galaxies.

In this work we aim to perform the first detailed study of the effect of dark energy on galactic scale using high resolution hydrodynamical simulations. Our study is an extension of the MaGICC project (Making Galaxies In a Cosmological Context) and we dubbed it DarkMaGICC. The MaGICC project has been quite successful in reproducing several properties of observed galaxies, including star formation rates and stellar masses (Brook et al. 2012; Stinson et al. 2013a), metals production and distribution (Stinson et al. 2012; Brook et al. 2013b), flat rotation curves and cored profiles (Macciò et al. 2012; Di Cintio et al. 2014) and disc properties as observed in the Milky-Way (Brook et al. 2013a; Stinson et al. 2013b).

We adopt the same set of numerical parameters describing the baryonic physics as in Stinson et al. (2013a), and perform high resolution hydrodynamical simulations with different dark energy backgrounds, to study the impact of Cosmology on galaxy properties. In the spirit this paper is very similar to the recent work by Herpich et al. (2014) that extended the MaGICC project to Warm Dark Matter cosmologies.

This paper is organized as follows. In Section 2 the cosmological models are described and compared with observational constraints. In Section 3 we introduce the numerical methods and implementations. In Section 4.1 we outline the results from our set of simulations and investigate the interplay between feedback and dark energy. Finally we draw conclusions in Section 5.

## 2 COSMOLOGICAL MODELS

For our project we have chosen four dynamical Dark Energy (dDE) models, each of which is consistent with WMAP7 data (Komatsu et al. 2011) at the two sigma level. All the models have at  $z = 0$ :  $\Omega_{b0} = 0.0458$ ,  $\Omega_{DM0} = 0.229$ ,  $H_0 = 70.2 \text{ km}^{-1} \text{ s}^{-1} \text{ Mpc}^{-1}$ ,  $\sigma_8 = 0.816$ ,  $n_s = 0.968$ , where these parameters are density parameters for baryons and dark matter, Hubble constant, root mean square of the fluctuation amplitudes and primeval spectra index.

Three of the cosmological models,  $\text{waCDM0}$ ,  $\text{waCDM1}$  and  $\text{waCDM2}$ , are based on a linear CPL parametrization (Chevallier & Polarski 2001 and Linder 2003) of the equation-of-state parameter  $w$

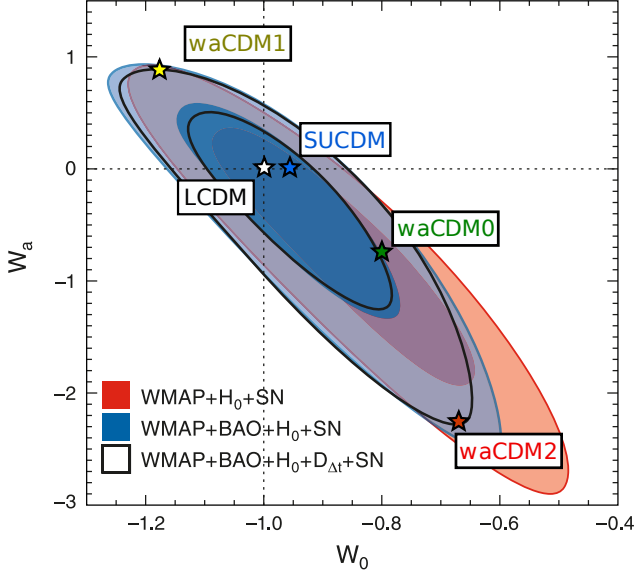
$$w(a) \equiv p(a)/\rho(a) = w_0 + (1 - a)w_a \quad (1)$$

In Table 1 we show the values we chose for  $w_0$  and  $w_a$  in each of the three cases.  $\text{waCDM0}$  is a model very close to  $\Lambda$ CDM as shown in Casarini et al. (2009), while  $\text{waCDM1}$  and  $\text{waCDM2}$ , already studied in Casarini et al. (2011a), are most distant in terms of  $w_a$  on the  $w_0$ - $w_a$  contour plot in Figure 1.

We have then also included a fourth cosmological model, which we called SUCDM, in which dark energy is described

**Table 1.** Parameters of the  $w$ aCDM cosmological models

	$w_0$	$w_a$
waCDM0 (green)	-0.8	-0.755
waCDM1 (yellow)	-1.18	0.89
waCDM2 (red)	-0.67	-2.28


**Figure 1.** Confidence contours of constraints for  $w_0$  and  $w_a$  from WMAP7. Each cosmological model is represented by a star. All of these models are *viable* models according to WMAP7 data. The star representing the SUCDM model is here shown only for comparison, but clearly its position on this plot holds only at  $z = 0$ , since its equation-of-state parameter  $w(a)$  cannot be described by the CPL parametrization.

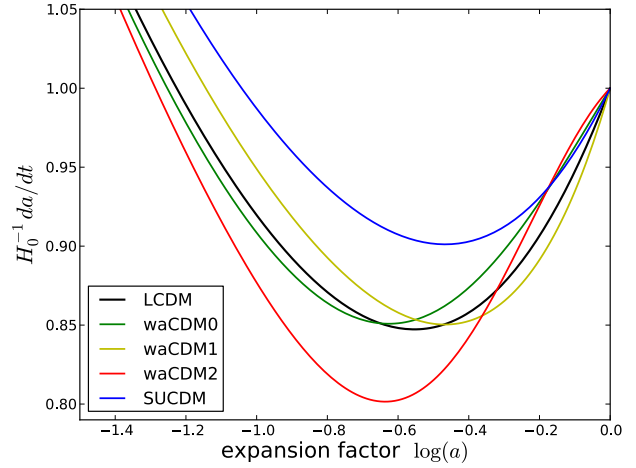
by a scalar field with a SUGRA (Super GRAvity) self-interacting potential of the form

$$V(\phi) = \frac{\Lambda^{4+\alpha}}{\phi^\alpha} \exp(4\pi G\phi^2) \quad (2)$$

where we chose  $\alpha = 2.9$  and  $\Lambda = 10$  GeV in agreement with Alimi et al. (2010).

In Figure 1 the two-sigma contours from WMAP7 in the  $w_a$ - $w_0$  plane are shown, and each cosmological model is represented by a triangle. It is important to note that *all* of these models are *viable* models according to WMAP7 data. The triangle representing the SUCDM model is here shown only for comparison, but clearly its position on this plot holds only at  $z = 0$ , since its equation-of-state parameter  $w(a)$  cannot be described by the CPL parametrization.

In order to show how the background evolution of these different cosmological models changes, in Figure 2 we show the expansion velocity of the universe in all the different chosen cosmologies. We chose to compare different cosmological models by normalizing them to the same  $\sigma_8$  today. With this choice, a model with a faster expansion will have to start producing structure earlier than a model with slower universe expansion. This means that statistically, the SUCDM model


**Figure 2.** Expansion velocities of the universe in units of the Hubble constant as a function of the scale factor. Different colors represent different cosmological models.

(blue) will show collapsed structures at an earlier epoch than the waCDM2 model (red), in order to compensate for the faster expansion of the universe. The earlier structure formation also leads to earlier accretion of the substructures onto the main halo. In turn, we expect that earlier accretion will lead to earlier star formation in the simulated galaxies.

### 3 NUMERICAL METHODS

#### 3.1 Initial Conditions and Dynamical Dark Energy generalization

We modified the initial condition generator GRAFIC-2 (Bertschinger 2001) such that we can generate initial conditions for a generic cosmological model once the evolution of the cosmological parameters are given as an input. Our implementation requires transfer functions for baryons and for dark matter at initial and final redshift, evolutions of the density parameters  $\Omega_i$ , linear growth factor  $D_+$  and  $f_\Omega$ , the logarithmic derivative of the growth factor with respect to the scale factor.

We have computed the transfer functions with a modified version of CAMB (Lewis & Bridle 2002) that allows us to account for dynamical dark energy scenarios. As the original code, GRAFIC-DE is able to generate zoomed initial conditions from a cosmological box.

At first we generate a uniform particle distribution in a 80 Mpc/h box with  $350^3$  particles. The initial conditions were evolved with the PKDGRAV tree-code (Stadel 2001), we then select a dark matter halo and we re-simulate it with PKDGRAV for the dark-matter-only runs and with GASOLINE Wadsley et al. (2004) for the hydrodynamical runs. The  $\Lambda$ CDM halos are chosen so that no structures are present in within three of their virial radii and the equivalent halos in the other cosmological models are then identified.

Both PKDGRAV and GASOLINE have been modified so that they can accept cosmological background evolutions as inputs. We have simulated three different galaxies, gal $\alpha$ , gal $\beta$ , gal $\gamma$ , and each of them was then run in all five cosmological models. In Table 2 we summarize the main propri-

**Table 2.** Physical properties of the selected galaxies for the respective  $\Lambda$ CDM cases. We show virial radius, virial mass (total mass), dark matter mass, gaseous mass and stellar mass, respectively calculated within one virial radius.

	$R_{\text{vir}}$ [kpc]	$M_{\text{vir}}$ [ $M_{\odot}$ ]	$M_{\text{DM}}$ [ $M_{\odot}$ ]	$M_{\text{gas}}$ [ $M_{\odot}$ ]	$M_{\star}$ [ $M_{\odot}$ ]
gal $\alpha$	240	$7.7 \times 10^{11}$	$6.8 \times 10^{11}$	$5.3 \times 10^{10}$	$4.5 \times 10^{10}$
gal $\beta$	227	$6.6 \times 10^{11}$	$5.8 \times 10^{11}$	$4.4 \times 10^{10}$	$3.9 \times 10^{10}$
gal $\gamma$	184	$3.4 \times 10^{11}$	$3.1 \times 10^{11}$	$2.7 \times 10^{10}$	$6.6 \times 10^9$

eties of the three galaxies in  $\Lambda$ CDM cosmology that we have chosen for this project. For all three galaxies the softening for gas and dark matter particles are respectively 0.45 and 1 kpc. Note that, for all galaxies, the SUGRA equivalents are always the most massive and, on the other hand, the waCDM2 are always the least massive.

### 3.2 Hydrodynamical Simulation

For the DarkMaGICC project we are using the same baryonic physics that was used in the MaGICC project (see Stinson et al. 2013a), based on the smoothed particle hydrodynamics (SPH) code GASOLINE (Wadsley et al. 2004). For further details on the physical processes implemented in GASOLINE please refer to Stinson et al. (2013a). Briefly, stars form from cool dense gas that has reached a temperature of  $T = 1.5 \times 10^4$  K and a density of  $9.6 \text{ cm}^{-3}$  following the Kennicutt-Schmidt Law with 10% efficiency of turning gas into stars during one dynamical time (Stinson et al. 2006). The stellar mass distribution in each star particle follows the Chabrier initial mass function (IMF), Chabrier (2003).

Massive stars explode as type II supernovae and deposit an energy of  $E_{\text{SN}} = 10^{51}$  ergs into the surrounding gas. Cooling for gas particles subject to supernova feedback is delayed based on the sub-grid approximation of a blast wave as described in Stinson et al. (2006).

Furthermore, radiation energy from massive stars is considered since molecular clouds are disrupted before the first supernova explosion (which happens after 4 Myr from the formation of the stellar population). We assume that 10% of the total radiation energy is coupled with the surrounding gas. The inclusion of this early stellar feedback reduces star formation before supernovae start exploding. Thus, after the early stellar feedback heats the gas to  $T > 10^6$  K, the gas rapidly cools to  $10^4$  K, which creates a lower density medium than if the gas were allowed to continue cooling until supernovae exploded. Stinson et al. (2013a) shows how this feedback mechanism limits star formation to the amount prescribed by the stellar-halo mass relationship at all redshifts. The code also includes metal cooling and metals can diffuse between gas particles as described in Shen et al. (2010).

The hydrodynamical simulations in *all* cosmological models have been run with the *same* feedback descriptions just mentioned. The main point of the work is not which of the many recently used feedback recipes best reproduced observations, but the impact of dynamical Dark Energy on galactic scales.

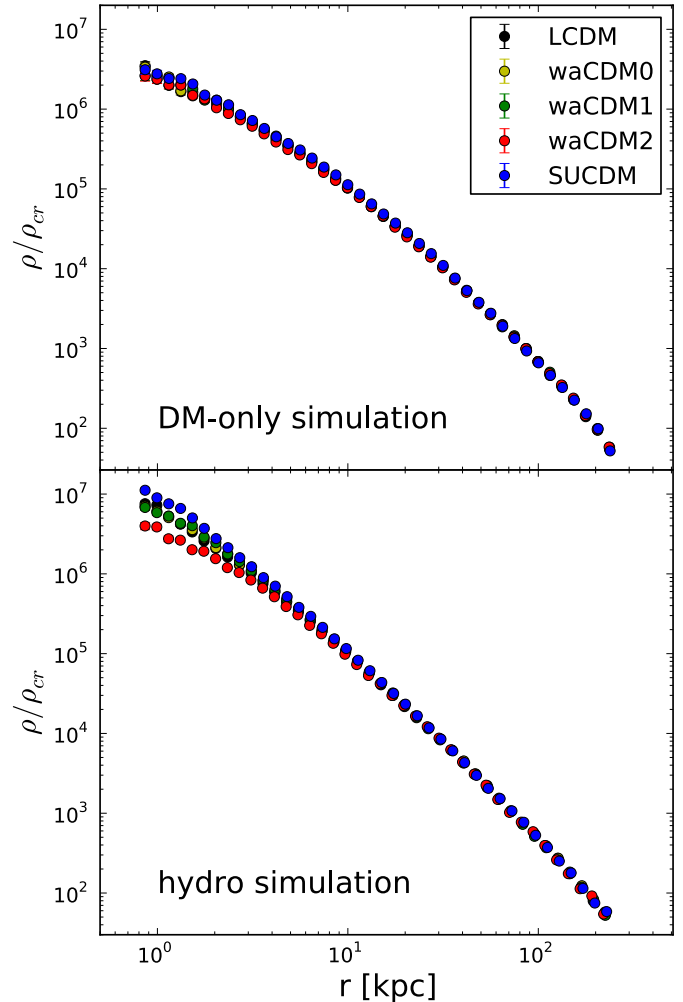


**Figure 3.** Radial density profile of gal $\alpha$  simulated in all five cosmological models, respectively in a dark matter only (upper panel) and in a hydrodynamical simulation (lower panel). We plot the density in units of critical density,  $\rho_{\text{crit}} = \frac{3H_0^2}{8\pi G}$  with  $G$  gravitational constant, as a function of the distance from the center of mass of the galaxy. Different colors represent different cosmological models.

## 4 RESULTS

Using hydrodynamical and dark matter only simulations, we present how gal $\alpha$ , gal $\beta$  and gal $\gamma$  evolved and their  $z = 0$  properties. These include the dark matter distribution, gas, star and total halo masses, star formation histories, baryonic matter distribution (rotation curves and surface brightness profiles), and the chemical enrichment of the galaxies.

### 4.1 Stellar and Halo Mass

Fig. 3 shows how the dark matter profiles of simulations with and without baryons compare in gal $\alpha$  for all different cosmological models. Gal $\beta$  and gal $\gamma$  show similar results. The four radial density profiles from the dark matter only simulations (top panel) are almost indistinguishable. This confirms previous findings from N-body simulations (see Section 1), i.e.

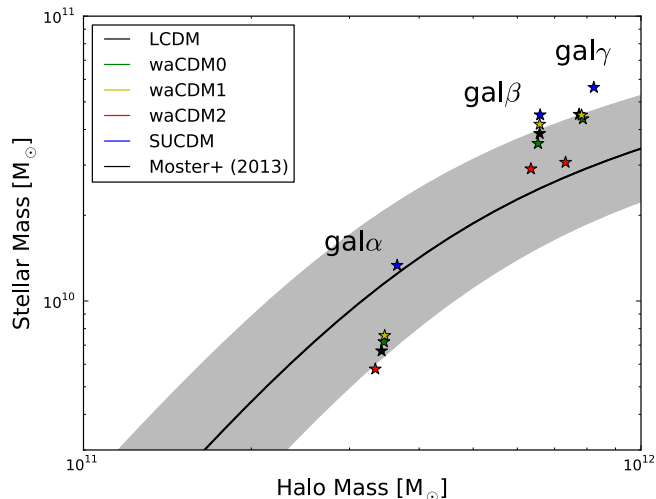


**Figure 4.** Stellar mass as a function of halo mass at  $z = 0$  for  $\text{gal}\alpha$ ,  $\text{gal}\beta$ ,  $\text{gal}\gamma$  simulated in all the different cosmologies.

that dark matter only simulations on galactic scales weakly depend on the dark energy model.

The lower panel of Fig. 3 shows the radial density profiles of dark matter in hydrodynamical simulations. In contrast to the dark matter only simulations, the density profiles vary depending on the dark energy model used.

Fig. 4 sets  $\text{gal}\alpha$ ,  $\text{gal}\beta$  and  $\text{gal}\gamma$  in the abundance matching plot at  $z = 0$ . The black line represents the prediction obtained by the abundance matching technique (see Moster et al. 2013), and the shaded area represents the errors on the prediction. The abundance matching prediction does not vary from  $\Lambda\text{CDM}$  to the other cosmologies since all cosmological models have the same value for  $\sigma_8$  at  $z = 0$ . While statistical conclusions are not possible because of the limited sample, the three galaxies show the same trend as a function of cosmology. By simply varying the cosmological model, the change among the three galaxies is of only a few percent in the dark matter mass, while the stellar mass almost doubles. Galaxies simulated in the  $\text{waCDM2}$  cosmology (red symbols) always make the least stars at  $z = 0$ , while the galaxies formed in the SUGRA cosmology (blue symbols) always make the most stars. Galaxies formed in a  $\Lambda\text{CDM}$  cosmology always lie in the middle. The hierarchy is in agreement with the behaviors of the cosmological background evolutions of these cosmological models (Fig. 2 and Section 1), since we expect more structures to be formed in a cosmological model that begins forming structures earlier.

## 4.2 Evolutions of the $M_\star - M_h$ relationship

Fig. 5 shows how the ratio of stellar mass and total mass evolve with expansion factor  $a = 1/(z + 1)$ . Each panel relates to a specific galaxy and the different colors describe each galaxy run in a different cosmology. Again, the black solid line represents the expected evolution for a  $\Lambda\text{CDM}$  model using the abundance matching technique. The predicted evolutions do change with the change in cosmology, but they all do not distance themselves significantly from the  $\Lambda\text{CDM}$  prediction. Hence, out of clarity, we have only plotted the  $\Lambda\text{CDM}$  predicted behavior from abundance match-

ing. As in the  $z = 0$  case, the  $M_\star - M_h$  trends for the galaxies simulated in different cosmologies are in agreement with the evolution of their cosmological backgrounds. In the SUCDM cosmology, we expect higher density perturbations to compensate for the faster expansion of the Universe. These higher density perturbations trigger a more efficient star formation (blue lines in Fig. 5). On the contrary, the  $\text{waCDM2}$  galaxy (red lines) always makes less stars throughout its evolution. The cosmological models  $\text{waCDM0}$  and  $\text{waCDM1}$  are not far apart from the  $\Lambda\text{CDM}$  model, in the  $w_a - w_0$  plane, thus we would expect galaxies that live in those models not to differ greatly from galaxies that live in the  $\Lambda\text{CDM}$  universe. This expectation is nicely reproduced for all three haloes.

As shown in Fig. 5 it is noticeable how both  $\text{gal}\alpha$  and  $\text{gal}\beta$  undergo a significant merger around  $a = 0.8$  which raises their star formation efficiency and increases their dark matter mass. The merger is visible also from the dark matter mass of the halos as a function of the scale factor. Fig. 6 shows a clear increase in the dark matter mass due to the accretion of a nearby satellite galaxy.

## 4.3 Star Formation Histories

Fig. 7 shows the star formation rate (SFR) as a function of physical time. At  $z = 0$  the different cosmological models show longer or shorter ages of the Universe because how much physical time elapses as the Universe expands depends on the choice of cosmology. The choice of showing the star formation in standard physical units gives more insight.

Fig. 7 shows how dark energy can suppress and delay star formation. Interestingly, the  $\text{waCDM2}$  cosmology (red lines) *delays* star formation, both in the case of  $\text{gal}\alpha$  and  $\text{gal}\beta$ . In all three galaxies the  $\text{waCDM2}$  cosmology drastically *suppresses* star formation until recent times.

As pointed out in Section 4.2, both  $\text{gal}\alpha$  and  $\text{gal}\beta$  undergo a merger. The merger event is clearly marked by the presence of a peak in the SFRs between 7 and 10 Gyrs (notice how the peak shifts in time according to the cosmological model). After the star formation burst due to the merger, both galaxies decrease their star formation activity due to the decrease in the amount of available cold gas. This is shown in Fig. 6, where we plot the evolution of the dark matter mass and the cool gas mass ( $T < 10^5$  K).

## 4.4 Rotation Curves

Different star formation histories reflect different matter distributions among the galaxy, as the rotation curves in Fig. 8 show. Galaxies with delayed star formation ( $\text{waCDM2}$  cosmology, red lines in Fig. 7) have flatter rotation curves than galaxies where star formation started earlier (SUCDM cosmology, blue lines), see Stinson et al. 2013a. Thus, a galaxy can have a flat or centrally peaked rotation curve based simply on the background cosmology in which it forms.

Centrally peaked rotation curves have long been the prime symptom of the overcooling problem in disk galaxy formation simulations, see Scannapieco et al. (2012). In the centers of halos the gas density becomes high enough that hot gas starts radiating and consequently cools. In such environments, the cooling process is unstable because, once the

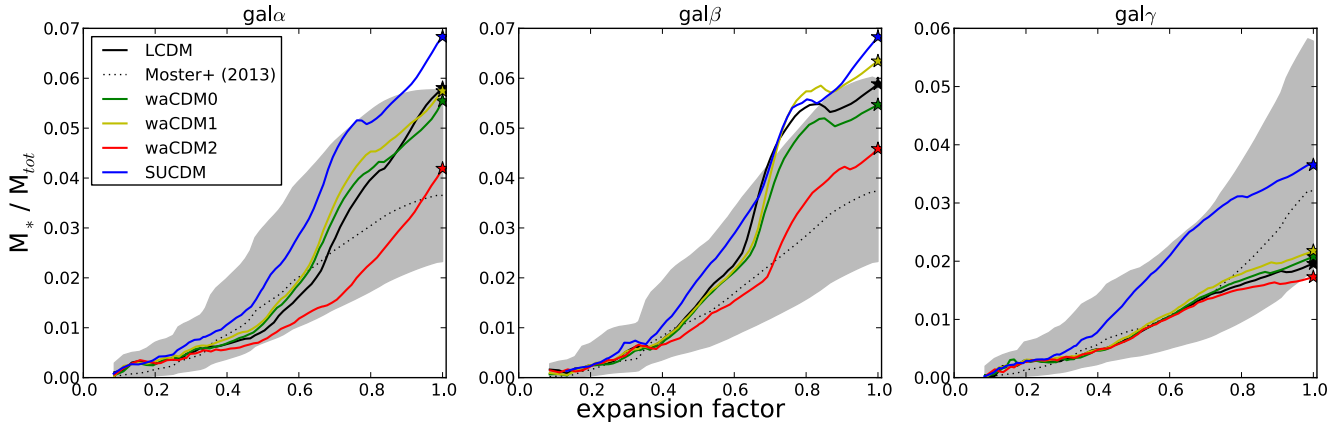


**Figure 5.** Evolutions of the stellar-halo mass relation as a function of expansion factor for  $\text{gal}\alpha$ ,  $\text{gal}\beta$  and  $\text{gal}\gamma$ .

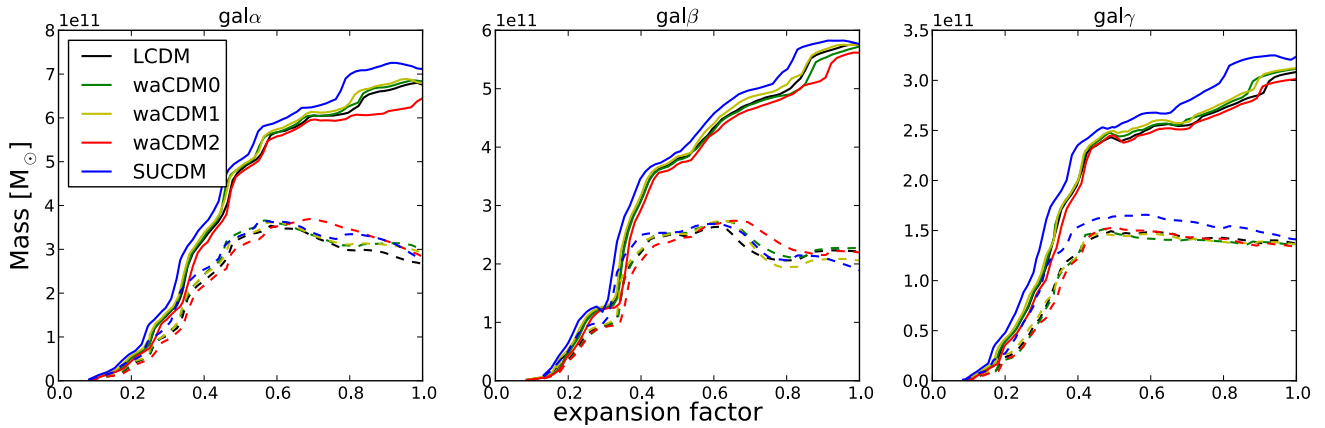


**Figure 6.** Evolution of the dark matter mass (solid lines) and gas mass (dashed lines) as a function of scale factor for the for  $\text{gal}\alpha$ ,  $\text{gal}\beta$  and  $\text{gal}\gamma$  in all different cosmological models. For an easier comparison, the gas mass was increased of a factor of five.

hot gas has cooled, it no longer pressure supports the surrounding gas, which then becomes denser and cools. Stars then form in excess and primarily in the central concentration, and they produce peaked rotation curves.

Most solutions have focused on adding energy from stars or AGN (Scannapieco et al. 2012). Stinson et al. (2013a) showed one solution based on stellar winds from massive stars (i.e. “early stellar feedback”). Our results show that also cosmology can have a considerable effect on flattening rotation curves.

This work shows that *simply* changing the evolutions of the dark energy equation of state *flattens* rotation curves of a considerable and definitely *observable* amount (i.e. more than 100 km/s in both  $\text{gal}\alpha$  and  $\text{gal}\beta$ ). Fig. 9 compares rotation curves for  $\text{gal}\alpha$  in dark matter only simulations (upper panel) and in SPH simulations (lower panel) for each cosmological model. The change is striking. While in the dark matter only case the cosmological models are almost indistinguishable, they become clearly distinguishable in the hydrodynamical simulations.

Stinson et al. (2013a) show that early stellar feedback is a key ingredient to simulate realistic disc galaxies. In particular, early stellar feedback can flatten rotation curves.

Unexpectedly, at  $z = 0$  the effect of early stellar feedback is comparable with the effect of dynamical dark energy.

#### 4.5 Disc Scale Lengths

Differences due to cosmologies are also visible in the surface brightness profiles at  $z=0$ , as Fig. 10 shows. Here we plotted only the two extreme cosmological models out of clarity. As seen in Section 4.3, waCDM2 cosmology (red lines) is able to suppress and delay star formation until low redshifts, when star formation finally starts to increase. In turn, a suppressed and delayed star formation affects the shapes of the surface brightness profiles, especially in the two most massive galaxies.  $\text{Gal}\alpha$  and  $\text{gal}\beta$  show steeper profiles in their inner regions (for further discussion on effects of delayed star formation on surface brightness profiles, see Stinson et al. 2013b).

The rest of the cosmological models do not significantly affect the profiles nor the scale lengths. As shown in the previous sections, the effect of cosmology seems to increase when the galaxy has a mass that is close to the peak of baryonic efficiency, and this is confirmed also when looking at the surface brightness profiles, where the effects of cosmology on  $\text{gal}\gamma$  are not significant.



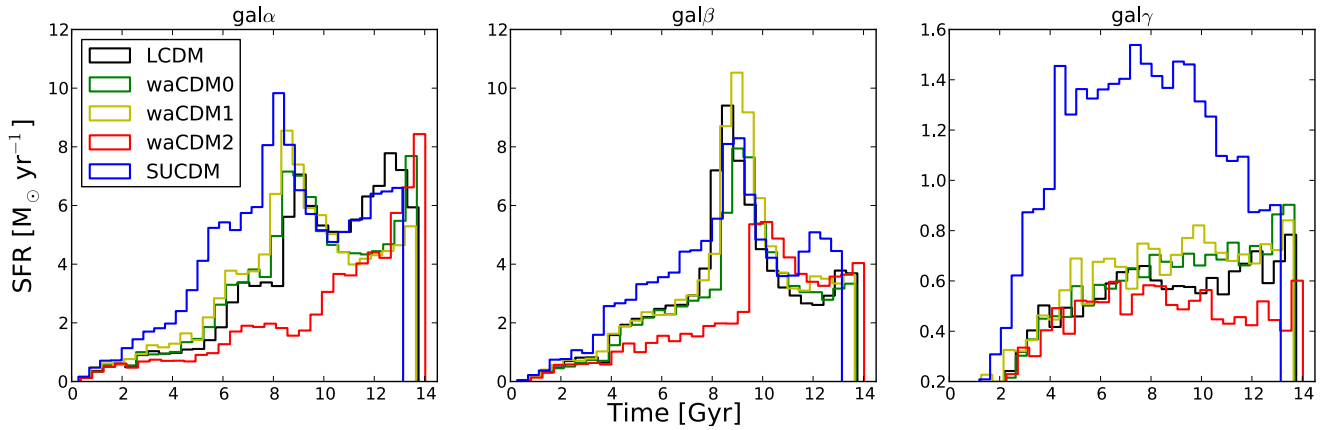


**Figure 7.** Star formation histories for  $\text{gal}\alpha$ ,  $\text{gal}\beta$  and  $\text{gal}\gamma$  in all the cosmological models.

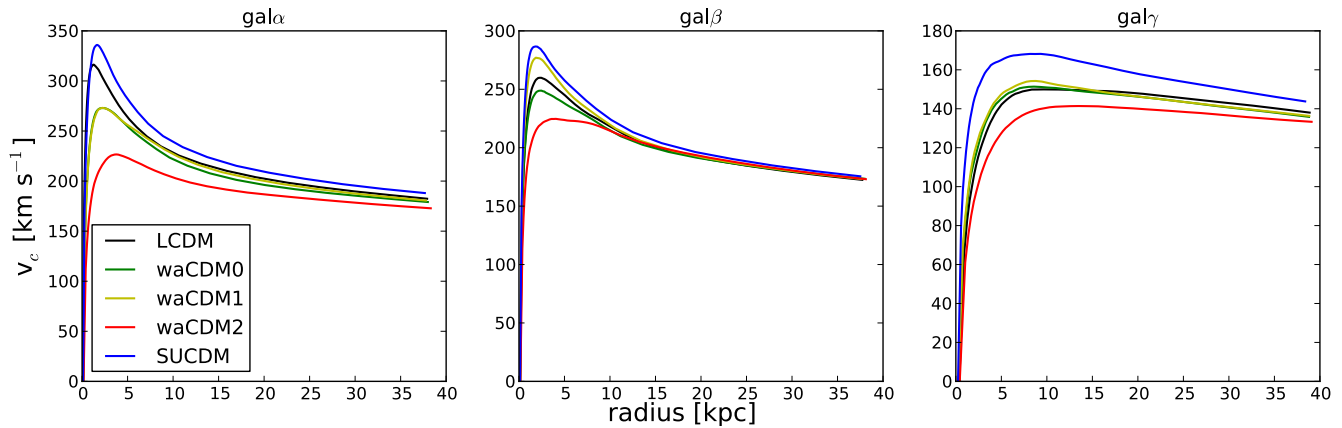


**Figure 8.** Rotation curves for  $\text{gal}\alpha$ ,  $\text{gal}\beta$  and  $\text{gal}\gamma$  in all the cosmological models.

#### 4.6 Feedback and cosmology, metallicity interplay

We showed that a model whose universe velocity expansion is slower compared to the one of  $\Lambda$ CDM (e.g. waCDM2, red lines) has a lower star formation till much later times, and on the other hand a model whose universe velocity expansion is faster than  $\Lambda$ CDM (e.g. SUGRA, blue lines) has a higher star formation at all redshifts (see Figure 7). We can trace back this difference to the fact that all five different cosmological models have the same  $\sigma_8$  today, because, in order for this to happen, structures in a SUGRA model (blue lines) have to start forming earlier. This implies that, at the starting redshift ( $z = 99$  for all simulations), the density perturbations that seeded structure formation had to be slightly bigger in the SUGRA model (blue lines) compared to the initial density perturbations in the waCDM2 model (red lines). Thus, stars will start forming earlier since more gas is accreted and cools.

These differences in the initial perturbations do not significantly affect properties of structures on galactic scales in dark matter only simulations. On the other hand, the interplay between cooling, metallicity and star formation not only helps differentiating between the cosmological models but also enhances their differences. To highlight the positive feedback star formation has on radiative cooling through

metal enrichment, the first three rows of Fig. 11 show the evolution of metallicity as a function of scale factor for three different regions of  $\text{gal}\alpha$  and  $\text{gal}\beta$ , a central 2 kpc sphere (“bulge”), a disk cylinder with radius 20 kpc and 6 kpc thickness (“disc”), and a sphere of the size of the  $R_{\text{vir}}$  (“halo”).

The waCDM2 model (red) exhibits the lowest metallicity in the bulge and disc throughout its evolution, which reflects its lower star formation rate and hence lower enrichment rate. The effect of increased metal enrichment is non-linear: the more star formation enriches gas, the faster the gas cools, and the more stars that subsequently form.

The halo metallicity of waCDM2 is also lower throughout most of the galaxy evolution, but becomes higher after  $a \sim 0.75$ , as its mean halo metallicity continues increasing while the metallicity in the other models starts to decrease or flatten out at that time. Both waCDM2 galaxies start to have more metallicity in the halo due to Supernova explosions being able to move the gas outside from the disc.

Comparing the trends for metallicity, cool gas (Fig. 11) and star formation rates (Fig. 7) as functions of scale factor, we find them in agreement. Because of the lower metallicity, the waCDM2 model (red line) ends up having the least amount of gas that has been able to cool and thus also makes the least amount of stars. Having used up a smaller amount of cold gas at earlier times increases the amount of cold gas

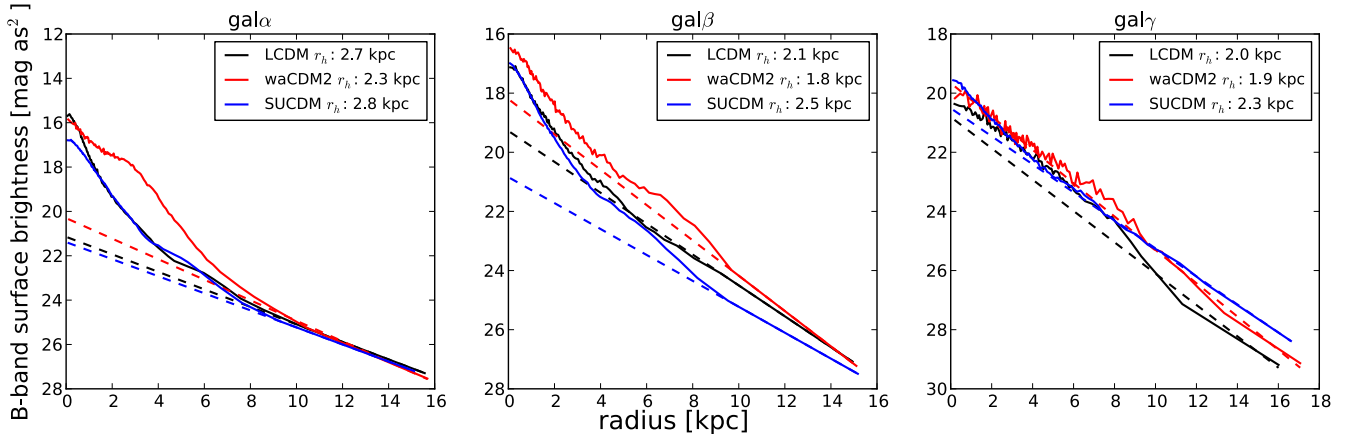


**Figure 10.** Disc scale lengths for  $\text{gal}\alpha$ ,  $\text{gal}\beta$  and  $\text{gal}\gamma$  for  $\Lambda$ CDM,  $w$ aCDM2 (red lines) and SUGRA (blue lines). For clarity, only these two models are shown.

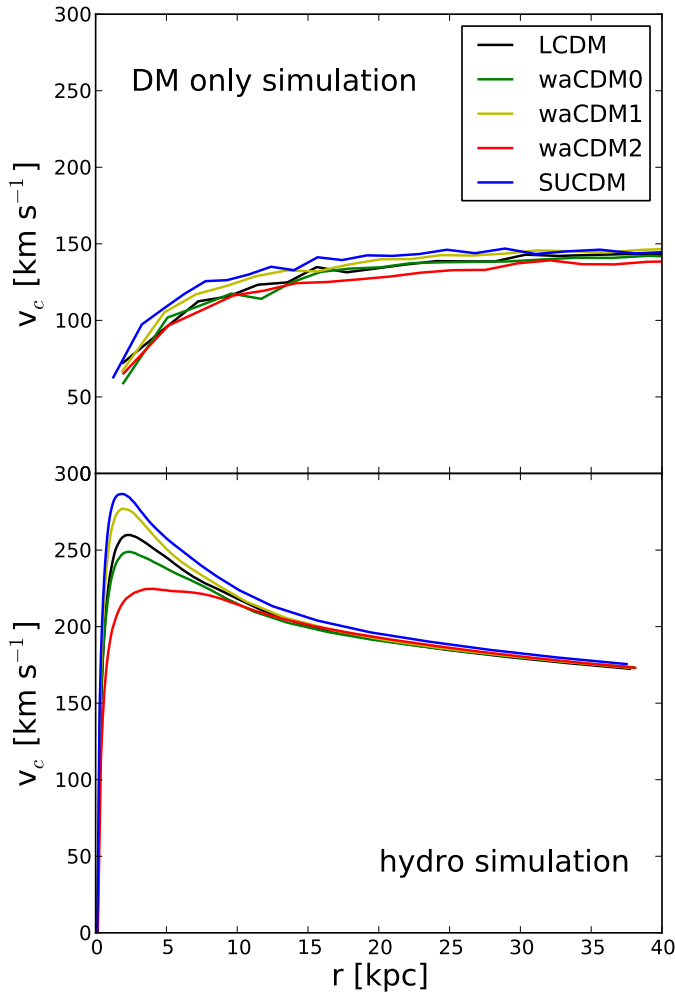


**Figure 9.** Rotation curve for  $\text{gal}\alpha$  in all different cosmological models, respectively in a dark matter only simulation (upper panel) and in a hydrodynamical simulation (lower panel).

left for star formation at late times. The presence of cool gas that has yet not formed stars can be seen in Fig. 11, where after  $a = 0.7$  the disc of the  $w$ aCDM2 galaxy has the most amount of cool gas compared to the galaxies in the other cosmological models. This is also the case for the galaxy halo, and this is probably due to the cooled gas moved by supernova explosions.

#### 4.7 Feedback–Dark Energy degeneracy

Along with dark energy having a profound effect on galaxy evolution, galaxy formation strongly depends on the feedback modeling. Stinson et al. (2013a) showed that pre-supernova feedback primarily suppresses star formation at early stages of evolution, which is similar to the evolution seen in the dark energy models that have the most delayed expansion. Thus, we wish to explore whether dark energy or stellar feedback has a greater effect at early times.

We select the  $w$ aCDM2 cosmology (red lines in previous plots), which showed the most star formation suppression and delay, and we re-simulate it with a range of stellar feedback strengths. We vary both the supernova feedback efficiency and the early stellar feedback separately.

First, the early stellar feedback is turned from 10% down to 0% efficiency with the standard  $10^{51}$  erg of supernova energy. Then, with 0 early stellar feedback, the supernova feedback strength is increased to 120% and 150%.

The left panel of Fig. 12 shows each of these variations implemented in the  $w$ aCDM2 model for  $\text{gal}\alpha$ . The stellar mass evolution shows a strong dependence on the early stellar feedback parameter. A decrease of 25% to 7.5% increases the final stellar mass 50% and moves most of the star formation from late to early times. All the simulations with less than 7.5% efficiency, but more than 0 early stellar feedback end with nearly the same final stellar mass. What is somewhat surprising is that the simulation with 0 early stellar feedback ends with less stellar mass than these intermediate feedback models. Stinson et al. (2013a) also saw this effect and found that it was due to the higher star formation efficiency at early times driving stronger outflows due to the greater supernova feedback. Thus, gas was driven to radii



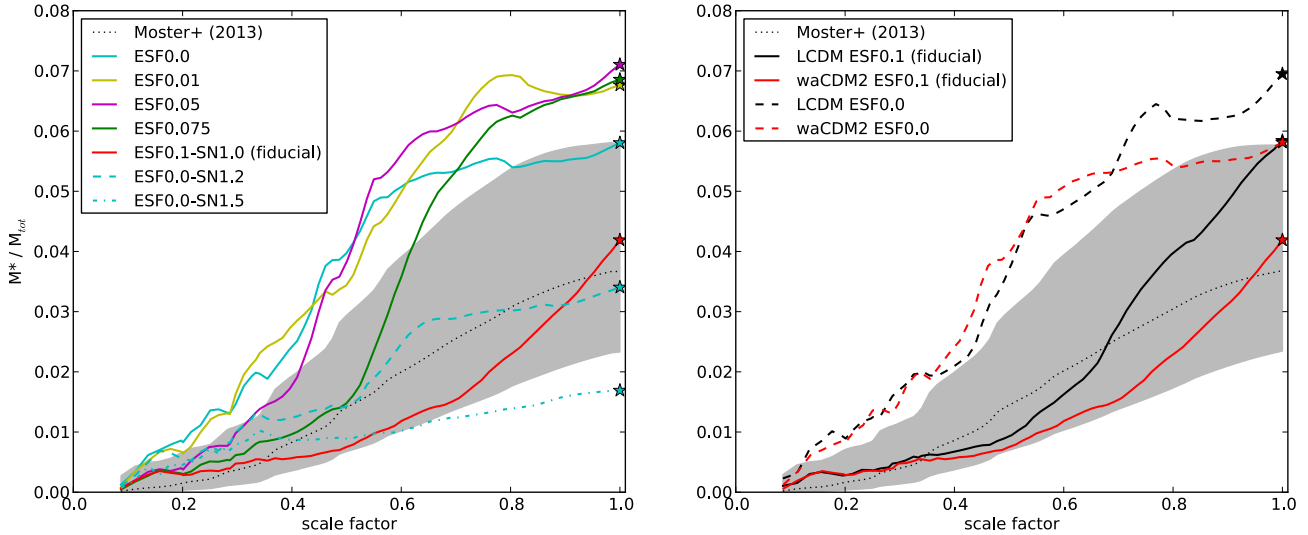


**Figure 12.** Evolution of stellar-halo mass relation with scale factor. We are now showing only the case of  $\text{gal}\alpha$ . In the left panel we have changed the feedback parameters for the  $\text{waCDM2}$  run. We have increased the early stellar feedback parameter from zero to the fiducial value (see Stinson et al. (2013a)) while keeping the SN parameter fixed to the fiducial value of 1.0 (solid lines). We then have changed the SN parameter while keeping the early stellar feedback fixed to zero (dashed and dash-dotted cyan lines). The dotted black line is the abundance matching prediction and the shaded area its errors. In the right panel we compare the effect of early stellar feedback with the effect of different cosmology,  $\Lambda\text{CDM}$  (red and black lines) and  $\text{waCDM2}$  (blue and red)

where it could not be reaccreted, whereas the early stellar feedback does not drive gas so far away.

Supernova feedback unambiguously decreases the amount of stars formed throughout the galaxy’s evolution, but can easily push the trends out of the expected behaviors from abundance matching techniques suggesting that Supernova feedback alone is not enough to reproduce realistic galaxies.

The right panel of Fig. 12 shows a comparison of the stellar mass-halo mass evolution of the  $\text{waCDM2}$  model (red lines) with the  $\Lambda\text{CDM}$  model (black lines) for  $\text{gal}\alpha$ . The models separate most notably at late times. The corresponding simulations with no early stellar feedback are shown in the dashed lines. They clearly show that cosmology has the strongest effect at late times (i.e. after  $a = 0.7$ ) and pre-SN feedback has the strongest effect at high redshift.

## 5 CONCLUSIONS

The intention of this work was to investigate for the first time the effect of dark energy on galactic scales in SPH simulations. We find that the dark energy modeling has an unexpected significant effect on galaxy formation, on the contrary of what is most commonly believed.

The experiment used a suite of SPH zoom-in cosmological simulations with masses of  $3.4 \times 10^{11} M_\odot$ ,  $6.6 \times 10^{11} M_\odot$  and  $7.7 \times 10^{11} M_\odot$ , in four dynamical dark energy models plus the reference  $\Lambda\text{CDM}$  model. The models all employed the *same* baryonic physics prescription. All dynamical dark energy models lay in within the two sigma contours given by WMAP7. We examined the dark matter distribution, gas, star and total halo masses, star formation histories, baryonic

matter distribution (rotation curves and surface brightness profiles), and the chemical enrichment of the galaxies.

Changing the dark energy evolution implies changing the expansion rate of the Universe, which in turn affects the accretion history. We show how the same galaxy evolved in different dark energy cosmologies does not present significant differences in dark matter only simulations, while in hydrodynamical simulations the galactic properties change greatly.

At  $z = 0$ , the stellar mass inside  $r_{\text{vir}}$  can vary by a factor of 2 depending on cosmology, while the dark matter mass only changes of a few percent. Thus baryons amplify differences between dark energy models, as the evolution of the stellar mass - halo mass ratio shows: by simply changing the dark energy parametrization stellar mass either decreases or increase of a factor of two throughout the whole galaxy evolution.

The reason why baryons amplify the differences among the various dynamical dark energy models lays on the non linear response of the hydrodynamical processes. Once the cosmological model introduces slightly different density perturbations, feedback processes enhances those differences by producing slightly more (or less) stars. More stars introduce more metals in the feedback cycle and more metals decrease the cooling time, which in turn allows gas to cool faster and produce even more stars. Through the highly non-linear response of baryons, dark energy models that would have been indistinguishable from  $\Lambda\text{CDM}$  on galactic scales show distinctive features in SPH simulations.

The distinctive features of dynamical dark energy become clear when looking at the star formation rates. We find that certain dark energy models are able to both delay and suppress star formation until recent epochs. The delay in

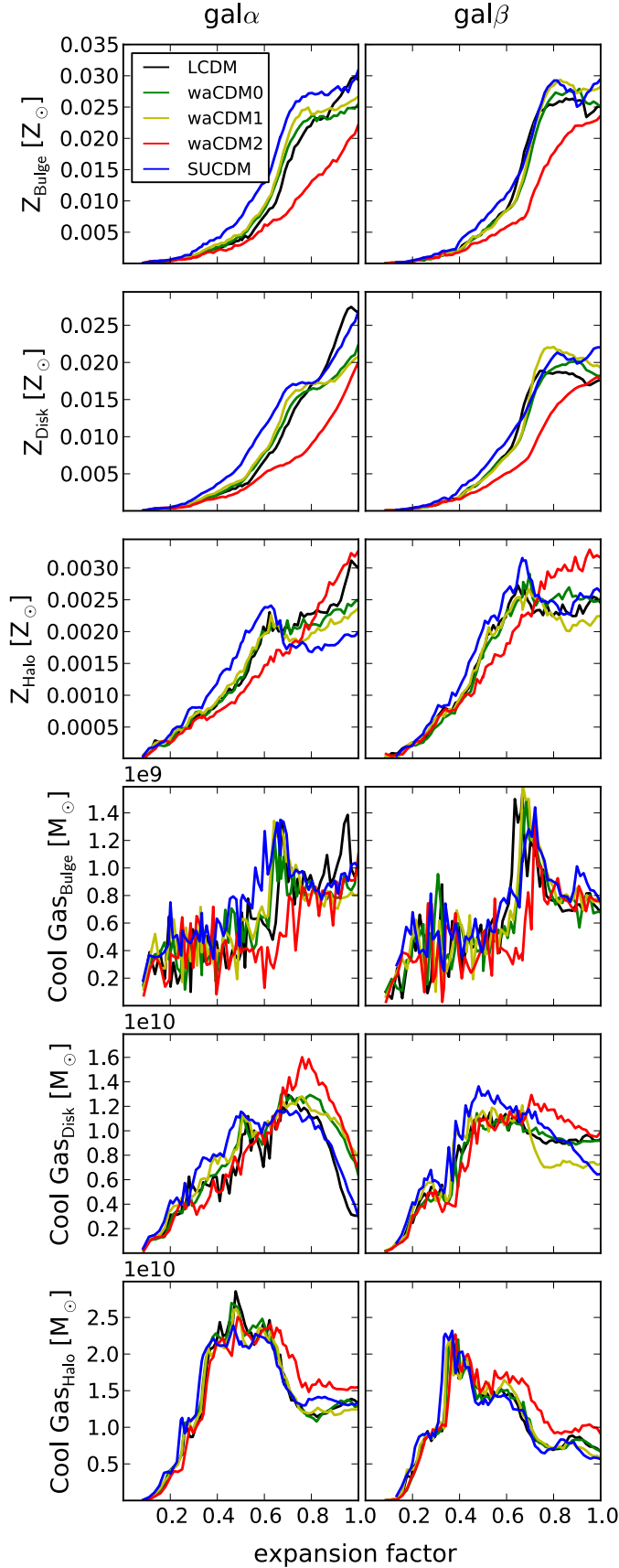


**Figure 11.** Mean metallicity in solar units and cool gas in solar masses ( $T < 10^5 \text{K}$ ) for  $\text{gal}\alpha$  and  $\text{gal}\beta$  as function of scale factor in “bulge”, “disc” and “halo”. Different colors represent different cosmological models.

star formation is then in turn responsible for the flattening of rotations curves, where we show a change of about 100 km/s in the two most massive galaxies we considered. Throughout the analysis, the least massive galaxy is the least sensitive to dark energy parametrization changes, in agreement with the fact that stellar feedback is most effective around  $10^{11} M_\odot$  (Di Cintio et al. 2014). The two most massive galaxies living in a slower expanding universe (waCDM2 model) have steeper surface brightness profiles due to their delayed star formation.

Finally we compare the effect of dynamical dark energy with the effect of baryonic feedback. We keep the cosmology fixed (waCDM2) and change the feedback parametrization. Provided that the Supernova feedback is kept constant, at late times the effect of dark energy is comparable to the effect of early stellar feedback (see Stinson et al. 2013a for details on feedback modeling). Even the degree at which stellar feedback is able to flatten rotation curves, is comparable to the effect of dark energy. We noted on the other hand, that in order to obtain the behavior suggested by abundance matching considerations at high redshifts, early stellar feedback had to be introduced since at high redshifts it has the most important effect compared to the dark energy modeling.

Having shown that the dark energy modeling has an important effect on galaxy formation and evolution, we would like to stress on the fact that, especially in the era of high precision cosmology, the details on dark energy do matter and certainly need further investigations.

## ACKNOWLEDGMENTS

The analysis was performed using the pynbody package (<http://code.google.com/p/pynbody>), which was written by Andrew Pontzen and Rok Roškar in addition to the authors. Luciano Casarini acknowledges the Brazilian research Institutions FAPES and CNPq for financial support. The numerical simulations used in this work were performed on the THEO cluster of the Max-Planck-Institut für Astronomie at the Rechenzentrum in Garching. And A.M. would like to acknowledge the support from the Sonderforschungsbereich SFB 881 “the Milky Way System” of the German Research Foundation (DFG). Greg Stinson received funding from the European Research Council under the European Union’s Seventh Framework Programme (FP 7) ERC Grant Agreement n. [321035].

## REFERENCES

- Agertz, O., Teyssier, R., & Moore, B. 2011, MNRAS, 410, 1391
- Alimi, J.-M., Füzfa, A., Boucher, V., et al. 2010, MNRAS, 401, 775
- Baldi, M. 2012, Physics of the Dark Universe, 1, 162
- Bartelmann, M., Dolag, K., Perrotta, F., et al. 2005, ApJ, 49, 199
- Bertschinger, E. 2001, ApJS, 137, 1
- Brook, C. B., Di Cintio, A., Knebe, A., et al. 2013a, ArXiv e-prints, arXiv:1311.5492

- Brook, C. B., Stinson, G., Gibson, B. K., et al. 2013b, ArXiv e-prints, arXiv:1306.5766
- Brook, C. B., Stinson, G., Gibson, B. K., Wadsley, J., & Quinn, T. 2012, MNRAS, 424, 1275
- Carroll, S. M., Press, W. H., & Turner, E. L. 1992, Annual Review of Astronomy and Astrophysics, 30, 499
- Casarini, L., Bonometto, S. A., Borgani, S., et al. 2012, Astronomy and Astrophysics, 542, A126
- Casarini, L., La Vacca, G., Amendola, L., Bonometto, S. A., & Macciò, A. V. 2011a, Journal of Cosmology and Astroparticle Physics, 3, 26
- Casarini, L., Macciò, A. V., & Bonometto, S. A. 2009, Journal of Cosmology and Astroparticle Physics, 3, 14
- Casarini, L., Macciò, A. V., Bonometto, S. A., & Stinson, G. S. 2011b, MNRAS, 412, 911
- Chabrier, G. 2003, The Publications of the Astronomical Society of the Pacific, 115, 763
- Chevallier, M., & Polarski, D. 2001, International Journal of Modern Physics D, 10, 213
- De Boni, C., Dolag, K., Ettori, S., et al. 2011, MNRAS, 415, 2758
- Di Cintio, A., Brook, C. B., Macciò, A. V., et al. 2014, MNRAS, 437, 415
- Dolag, K., Bartelmann, M., Perrotta, F., et al. 2004, Astronomy and Astrophysics, 416, 853
- Fedeli, C., Dolag, K., & Moscardini, L. 2012, MNRAS, 419, 1588
- Fontanot, F., Puchwein, E., Springel, V., & Bianchi, D. 2013, ArXiv e-prints, arXiv:1307.5065
- Fontanot, F., Springel, V., Angulo, R. E., & Henriques, B. 2012, MNRAS, 426, 2335
- Governato, F., Willman, B., Mayer, L., et al. 2007, MNRAS, 374, 1479
- Grossi, M., & Springel, V. 2009, MNRAS, 394, 1559
- Guedes, J., Callegari, S., Madau, P., & Mayer, L. 2011, ApJ, 742, 76
- Herpich, J., Stinson, G. S., Macciò, A. V., et al. 2014, MNRAS, 437, 293
- Jing, Y. P., Zhang, P., Lin, W. P., Gao, L., & Springel, V. 2006, ApJL, 640, L119
- Klypin, A., Macciò, A. V., Mainini, R., & Bonometto, S. A. 2003, ApJ, 599, 31
- Komatsu, E., Smith, K. M., Dunkley, J., et al. 2011, ApJS, 192, 18
- Kuhlen, M., Strigari, L. E., Zentner, A. R., Bullock, J. S., & Primack, J. R. 2005, MNRAS, 357, 387
- Lewis, A., & Bridle, S. 2002, Phys. Rev., D66, 103511
- Linder, E. V. 2003, Physical Review Letters, 90, 091301
- Linder, E. V., & Jenkins, A. 2003, MNRAS, 346, 573
- Macciò, A. V., Stinson, G., Brook, C. B., et al. 2012, ApJL, 744, L9
- Marinacci, F., Pakmor, R., & Springel, V. 2013, ArXiv e-prints, arXiv:1305.5360
- Moster, B. P., Naab, T., & White, S. D. M. 2013, MNRAS, 428, 3121
- Navarro, J. F., Frenk, C. S., & White, S. D. M. 1997, ApJ, 490, 493
- Perlmutter, S., Aldering, G., Goldhaber, G., et al. 1999, ApJ, 517, 565
- Puchwein, E., Bartelmann, M., Dolag, K., & Meneghetti, M. 2005, Astronomy and Astrophysics, 442, 405
- Riess, A. G., Filippenko, A. V., Challis, P., et al. 1998, The Astronomical Journal, 116, 1009
- Robertson, B., Bullock, J. S., Cox, T. J., et al. 2006, ApJ, 645, 986
- Rudd, D. H., Zentner, A. R., & Kravtsov, A. V. 2008, ApJ, 672, 19
- Scannapieco, C., Wadepuhl, M., Parry, O. H., et al. 2012, MNRAS, 423, 1726
- Stadel, J. G. 2001, PhD thesis, University of Washington
- Stinson, G., Seth, A., Katz, N., et al. 2006, MNRAS, 373, 1074
- Stinson, G. S., Brook, C., Macciò, A. V., et al. 2013a, MNRAS, 428, 129
- Stinson, G. S., Brook, C., Prochaska, J. X., et al. 2012, MNRAS, 425, 1270
- Stinson, G. S., Bovy, J., Rix, H.-W., et al. 2013b, MNRAS, 436, 625
- van Daalen, M. P., Schaye, J., Booth, C. M., & Dalla Vecchia, C. 2011, MNRAS, 415, 3649
- Wadsley, J. W., Stadel, J., & Quinn, T. 2004, New Astronomy, 9, 137
- Weinberg, S. 1989, Reviews of Modern Physics, 61, 1
- White, S. D. M. 1976, MNRAS, 177, 717
- Xia, J.-Q., Li, H., & Zhang, X. 2013, Phy.Rev.D, 88, 063501
- Xia, J.-Q., Zhao, G.-B., Feng, B., Li, H., & Zhang, X. 2006, Phy.Rev.D, 73, 063521
- Zhan, H., & Knox, L. 2004, ApJL, 616, L75

This paper has been typeset from a  $\text{\LaTeX}$  file prepared by the author.